Pressure was controlled at around 50 K, and curves of resistance versus temperature were obtained at fixed pressures (3.5–48 GPa; Fig. 2). At pressures of 3.5 and 23 GPa, the measured resistance showed a normal metallic behaviour. The residual resistance increased with compression, which could be explained by thinning of the sample and possible chemical reactions at the contact point between the sample and the electrodes. At a pressure of 35 GPa, a drop of resistance was observed at around 13 K, and the onset temperature of the drop shifted slightly to higher temperature at 36 GPa. At 48 GPa (run no. 2), the width of the resistance drop increased and the onset temperature reached 20 K (Fig. 2a). The loss of resistance (50%) suggested that the drop was caused by the superconducting transition. Figure 3 shows the magnetic field dependence of the resistance drop at 34 GPa (run no. 3), which is strong evidence for the superconducting transition; the drop shifted to lower temperature when the magnetic field was applied, and was fully suppressed above 3 T. Observation of the Meissner signal is indispensable for proving the existence of superconductivity, but we had experimental difficulties in performing magnetic measurements with the gas-controlled DAC, and have not obtained this signal. After releasing the pressure, the sample showed its original reflection of light, which indicated that chemical reaction was negligible during the present experiments. We conclude that the drop of resistance is due to the onset of superconductivity of Li.

Figure 4 shows the pressure dependence of the superconducting onset temperature of Li observed in four different runs (nos 1–4). Data are scattered, but the onset temperature clearly shows (on average) a rise with pressure. Lin and Dunn[5] had previously reported high-pressure and low-temperature electrical resistance measurements on Li, and observed a drop of resistance at around 7 K in a similar pressure region to our results. Although they concluded that this drop of resistance was caused by a phase transition, which could include (as they tentatively proposed) the onset of superconductivity, here we suggest the resistance drop observed by these workers was indeed likely to have been from superconductivity. The present result establishes that compressed Li is a superconductor.

According to theoretical predictions[7,8] we may be able to achieve a T_c higher than 20 K on further compression. High-pressure investigations of Li, the first superconducting element of the periodic table, should help the understanding both of the fundamental properties of metals, and of the possible room-temperature superconductivity in metallic hydrogen[2]. □

Received 11 June; accepted 26 August 2002; doi:10.1038/nature01098.

1. Bardeen, J., Cooper, L. N. & Schrieffer, J. R. Theory of superconductivity. *Phys. Rev.* **108,** 1175–1204 (1957).
2. Richardson, C. F. & Ashcroft, N. W. High temperature superconductivity in metallic hydrogen: Electron-electron enhancements. *Phys. Rev. Lett.* **78,** 118–121 (1997).
3. Allen, P. B. & Cohen, M. L. Pseudopotential calculation of the mass enhancement and superconducting transition temperature of simple metals. *Phys. Rev.* **187,** 525–538 (1969).
4. Richardson, C. F. & Ashcroft, N. W. Effective electron-electron interactions and the theory of superconductivity. *Phys. Rev. B* **55,** 15130–15145 (1997).
5. Lin, T. H. & Dunn, K. J. High-pressure and low-temperature study of electrical resistance of lithium. *Phys. Rev. B* **33,** 807–811 (1986).
6. Neaton, J. B. & Ashcroft, N. W. Pairing in dense lithium. *Nature* **400,** 141–144 (1999).
7. Hanfland, M., Syassen, K., Christensen, N. E. & Novikov, D. L. New high-pressure phase of lithium. *Nature* **408,** 174–178 (2000).
8. Christensen, N. E. & Novikov, D. L. Predicted superconductive properties of lithium under pressure. *Phys. Rev. Lett.* **86,** 1861–1864 (2001).
9. Hanfland, M., Loa, I., Syassen, K., Schwarz, U. & Takemura, K. Equation of state of lithium to 21 GPa. *Solid State Commun.* **112,** 123–127 (1999).

Acknowledgements We thank H. Goto for technical support in machining the pit-anvils. This work was supported by a Grant-in-Aid for COE (Center of Excellence) Research and Scientific Research from the Ministry of Education, Culture, Sports, Science and Technology of Japan.

Competing interests statement The authors declare that they have no competing financial interests.

Correspondence and requests for materials should be addressed to K.S. (e-mail: kshimizu@mp.es.osaka-u.ac.jp).

Propagation of the polyamorphic transition of ice and the liquid–liquid critical point

Osamu Mishima & Yoshiharu Suzuki

Advanced Materials Laboratory (AML), National Institute for Materials Science (NIMS), 1-1 Namiki, Tsukuba, 305-0044 Japan

Water has a rich metastable phase behaviour that includes transitions between high- and low-density amorphous ices, and between high- and low-density supercooled liquids. Because the transitions occur under conditions where crystalline ice is the stable phase, they are challenging to probe directly. In the case of the liquids, it remains unclear[1] whether their mutual transformation at low temperatures is continuous[2,3], or discontinuous[4,5] and terminating at a postulated second critical point of water that is metastable with respect to crystallization. The amorphous ices are more amenable to experiments[6–8], which have shown that their mutual transformation is sharp and reversible. But the non-equilibrium conditions of these studies make a firm thermodynamic interpretation of the results difficult. Here we use Raman spectroscopy and visual inspection to show that the transformation of high-density to low-density amorphous ices involves the propagation of a phase boundary—a region containing a mixture of both ices. We find that the boundary region becomes narrower as the transformation progresses, and at higher transformation temperatures. These findings strongly suggest that the polyamorphic ice transition is discontinuous; a continuous transformation should occur uniformly over the entire sample[9]. Because the amorphous ices are structurally similar to their supercooled liquid counterparts, our results also imply that the liquids transform discontinuously at low temperatures and thus support the liquid–liquid critical-point theory[4,5].

We used pressure-induced amorphization of deionized H_2O ice at ~1 GPa, 77 K, to obtain high-density amorphous ice (HDA). The sample was then heated at 1.5 GPa to 150 K at ~3 K min^{-1} to make a large homogeneous HDA block; this was then 'recovered' at 100 kPa, 77 K (refs 10–12), yielding 'as-recovered' HDA as a transparent solid with few cracks.

A lump of the 'as-recovered' HDA, 1–2 mm in size, was placed at 77 K in a hole in an indium block attached to a cryostat, and heated in vacuum at 0.5 K min^{-1} to the annealing temperature T_{anneal}. The sample was kept at this temperature for about 3–3.5 h, and then cooled to 25 K; throughout this procedure, microscopic Raman spectra were taken to identify the ice phases[13] of the sample. The heating–annealing–cooling sequence was then repeated using a higher T_{anneal}.

Annealing (ageing) at T_{anneal} releases excessive stress: the HDA structure changes gradually and irreversibly, until the changes gradually cease with time[14] as evident from the Raman spectra and a decrease in the heat evolved from HDA per unit time (not shown). The Raman peak frequency of the annealed HDA sample changes with temperature almost reversibly between T_{anneal} and 25 K at a rate similar to that of low-density amorphous ice (LDA) and ice Ih (ref. 15), indicating that its structure is stable below T_{anneal} (ref. 14).

The Raman spectra of the sample at 25 K after the 3–3.5 h annealing at different T_{anneal} are shown in Fig. 1, and the corresponding peak frequencies, relative peak intensities, and estimated specific volumes at T_{anneal} are shown in Fig. 2. The HDA structure relaxes on annealing at ~90–115 K, and HDA transforms to LDA at $115 \pm \sim 0.5$ K, in agreement with previous results[12,16–18]. Although the transformation from HDA into LDA is associated with heat

© 2002 Nature Publishing Group

release[16], we believe that this does not lead to any significant heating of the sample itself because the transformation proceeds slowly.

Although the peak frequency and the specific volume of HDA change increasingly as T_{anneal} approaches 115 K (Fig. 2), the Raman spectra exhibit a common, broad profile (Fig. 1). The profiles measured at several different points on the surface of a given relaxed HDA sample are always identical within experimental error; any stresses remaining must therefore be homogeneously distributed throughout the HDA sample. Annealing to temperatures less than 115 K is accordingly accompanied by uniform sample swelling that causes no cracks; annealing at 115 K, in contrast, results in heterogeneous swelling and cracking, belying a monotonous change[14] to LDA.

The 25-K spectra of HDA annealed near 112 K (Fig. 1) are, within experimental error, identical to the 25-K spectra[13,19] of HDA samples that are not initially heat-treated at 1.5 GPa and also not annealed, indicating that these samples have similar structures, even though they differ subtly[12]. As annealing of HDA at 112 K at 100 kPa and heating HDA to 150 K at 1.5 GPa induces a gradual change to another HDA, their structures appear to change mutually and continuously. This suggests that different HDA states lie within the same HDA megabasin in configuration space[10].

The temporal evolution of the spatial distribution of the different ice states during annealing near 115 K is illustrated in Fig. 3. The HDA-to-LDA transformation starts in the left part of the ice sample and propagates to the right, accompanied by an increase in sample volume from left to right. The Raman spectra of the left part of the ice sample shown in Fig. 3b are similar to the Raman spectrum of LDA, whereas spectra taken of the right part of the sample resemble the HDA spectrum. The region between the LDA and HDA phases shows continuously changing intermediate spectra, which can be expressed as a linear combination of the spectra of HDA and LDA (Fig. 4). We classify these ice states by the fraction of the HDA component, α (see Fig. 4 legend for a full definition) and show in the right-hand panels of Fig. 3 how α changes along a line in the transformation direction (indicated by the X–X′ arrow in the left panels). The slope of α in the intermediate-state region (the slope of the broken lines in the right panels in Fig. 3) becomes steeper with time and, hence, the boundary region separating HDA from LDA narrows gradually. This suggests that the intermediate state changes more quickly to LDA than HDA changes to the intermediate state—a phase-separating behaviour. Large cracks, indicative of severe stress, appear mainly in the direction perpendicular to the transformation direction (Fig. 3). The high density of cracks in the right part of the ice sample correspond with a particularly steep slope in α observed at that location, suggesting that crack density correlates with the broadness of the boundary region.

In a separate experiment, we partly transformed a sample at 115 K and then kept it at a lower temperature of 111 K and monitored the changes of α along a line in the transformation direction. As illustrated in Fig. 5, the values of α in the left part of the sample, left of point P, decrease over time as the corresponding intermediate states transform into LDA. In contrast, HDA states to the right of this point remain unchanged. This behaviour clearly illustrates that the partially transformed sample segregates into HDA and LDA regions separated by a crack at P. Upon re-heating, the remaining HDA starts to change to the intermediate state (Fig. 5e). The data also show that the phase transformation of HDA to LDA, once initiated at 115 K, triggers complete transformation of the affected sample part, even at 111 K. This 'over-heating' effect is comparable to the 'over-depressurization' of the decompression-induced HDA-to-LDA transformation around 135 K, where the phase transformation, once it has begun, continues at a higher pressure (the transition b in Fig. 2 of ref. 8). The behaviour is consistent with the observed 'coexistence' of HDA and LDA during the phase transformation[12,20], which must therefore be discontinuous.

We used higher transformation temperatures to study the effect of temperature on the broadness of the boundary region. After annealing at 108–110 K for ~20 h and confirmation via Raman spectra that the HDA sample was in a state just before the transformation, we rapidly (~10 K min^{-1}) heated the sample and then kept it at a constant temperature between 115 K and 131 K. The transformation to LDA, once it starts, propagates more quickly at higher temperatures, leaving dense major and fine cracks. The transformation completes in ~5 h at

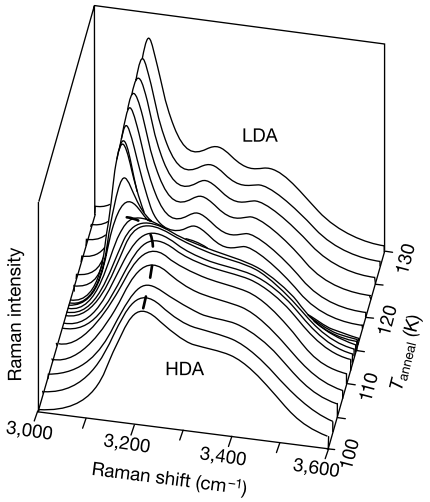

Figure 1 Changes in the Raman spectrum of a high-density amorphous ice sample during annealing at different temperatures T_{anneal}. Total intensity between 2,800 and 3,650 cm^{-1} in each spectrum is normalized. We measure the spectra to ± ~ 2 cm^{-1} at 25 K using an argon-ion laser (wavelength 488.0 nm); the laser power in a spot (~20 μm diameter) on the sample is ~10 mW. Sample temperature is controlled to ± ~ 0.1 K. HDA and LDA, high-density and low-density ice, respectively.

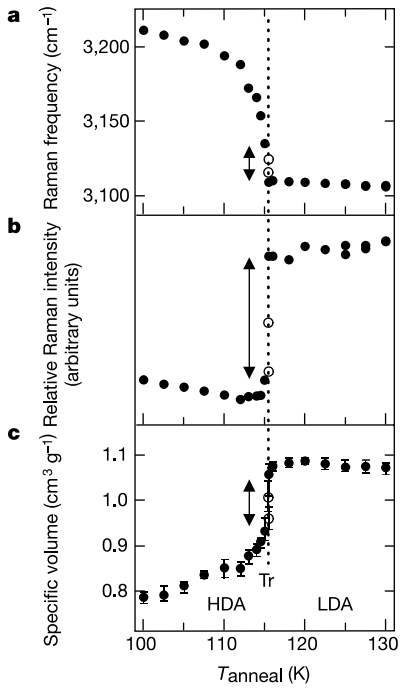

Figure 2 Changes in properties of Raman spectra induced by annealing of amorphous ice at different temperatures. **a**, Raman peak frequency; **b**, relative Raman peak intensity; and **c**, specific volume. Discontinuity at the transformation (Tr) is shown by gaps (arrows). Open circles correspond to the intermediate states at Tr. The specific volume is obtained by observing the sample surface with video equipment. We measure the length between several fixed points on the surface, raise it to the third power to obtain temporary volume, and estimate the specific volume to ~2% by calibrating the volume above 150 K with the specific volume of ice Ih or ice Ic.

© 2002 Nature Publishing Group

115 K and in ~0.03 s at 131 K. Raman spectra of a sample transforming at 123 K yield a steep slope of α in an apparently connected part of the sample that soon cracks; the slope is comparable to the steep slope measured for the sample of Fig. 3d.

Because of the speed of the transformations at higher temperatures, Raman measurements are not feasible, and we therefore used video equipment to observe the crack formation (or the volume evolution) during the transformations. Above ~132 K the transformation occurs within a single video frame (0.03 s)—making it too fast to observe the propagation. Owing to the variety of transformation directions, sudden crack formation and lack of *in situ* identification of the intermediate states, we have to repeat our observations dozens of times to obtain a meaningful result. We find that the boundary region between the cracked transformed part of the sample and the uncracked and untransformed part of the sample appears more distinct at higher temperatures (Fig. 6), suggesting that the boundary region is narrower, or similar, in width to the boundary region appearing in low-temperature transformations. This is further supported by the appearance of dense major cracks, which suggest narrow boundary regions (Fig. 3). The propagation and the probable narrowing of the boundary region indicate the relative stability of HDA even at high temperatures.

The presence of a boundary region in partly transformed samples argues for the HDA–LDA transformation having a first-order-like nature[9], given that continuous structural relaxation of HDA only at the boundary to the LDA region seems very unlikely. In fact, we observe that HDA relaxation always occurs uniformly and essentially without causing cracking, even in cases where quick and large volume expansion accompanies the relaxation. For example, when we heat 'as-recovered' 77-K HDA at ~20 K min^{-1}, it swells uniformly by 3–5 vol.% within a few seconds just before the transformation to LDA starts to propagate through the sample. The rate of this initial volume expansion is much higher than the rate of the volume expansion accompanying the HDA–LDA transformation at 115 K, yet the relaxation occurs uniformly and without causing cracks. Stresses heterogeneously distributed in HDA must therefore be able to quickly relax and spread uniformly through the sample. Moreover, if the boundary region appearing during the HDA–LDA transformation were caused by relaxation, it should broaden at higher temperatures because structural relaxation processes are usually more uniform higher temperatures; in contrast and as discussed above, we see evidence for narrowing of the boundary

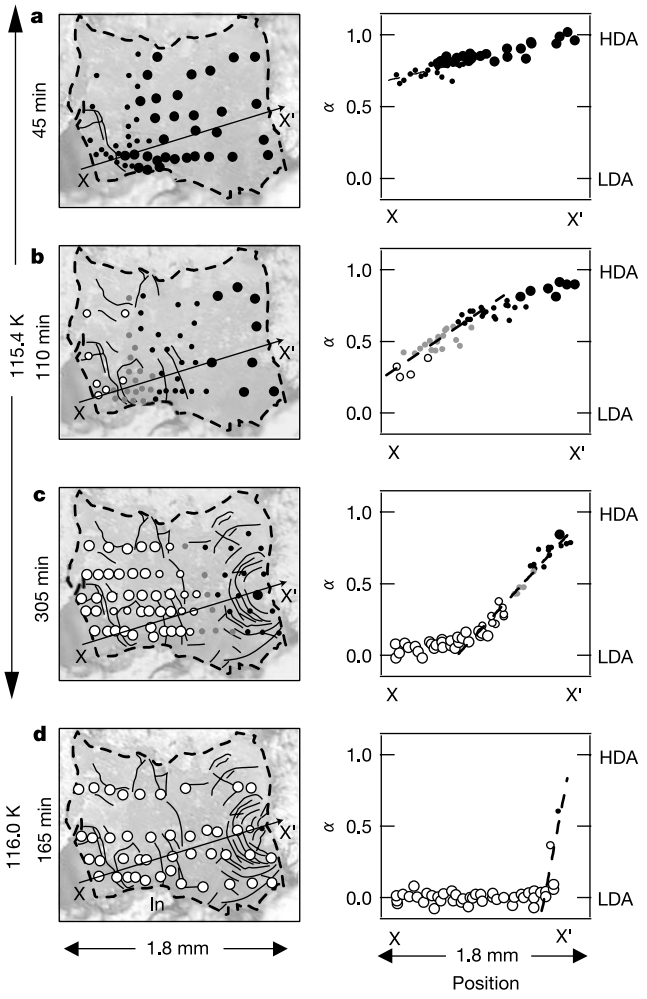

Figure 3 The transformation of HDA to LDA as a function of time. Time given on the left is that elapsed after annealing has started at 115.4 K (**a**–**c**) or 116 K (**d**). We suspend annealing by cooling the ice sample to 25 K, and then measure the Raman spectra at the points indicated on the sample (inside the broken lines) in an indium holder (In). Thin lines, observed major cracks. The surface state at each point is classified, and indicated by the appropriate dot. $\alpha > 0.8$, large black (HDA-like); $0.8 > \alpha > 0.6$, small black; $0.6 > \alpha > 0.4$, grey; $0.4 > \alpha > 0.2$, small white; $0.2 > \alpha$, large white (LDA-like), allowing for experimental uncertainties of α, $\pm \sim 0.1$. Arrow X–X′, direction of transformation. Graphs (right) show the progress of α along the line parallel to the arrow. Intermediate states (as mentioned in Fig. 4) are defined as those with $\alpha = 0$–1. Broken lines, slopes of α.

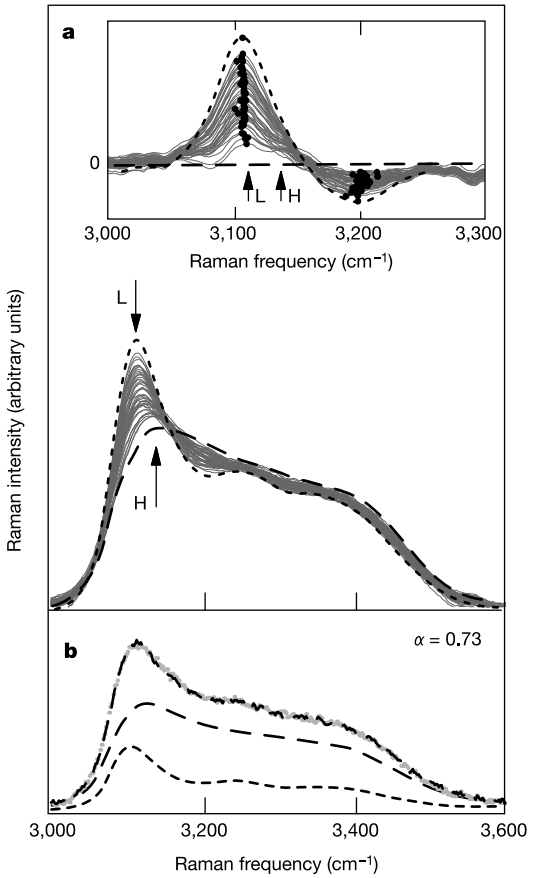

Figure 4 Raman spectra of an intermediate state at 25 K. **a**, All the spectra collected on the sample pictured in Fig. 3b. Inset, the difference in intensity between each spectrum and the HDA spectrum (just before the transformation starts to propagate). Note the isosbestic points and the same peak frequencies in the inset (black points). The arrows, L (3,112 $\pm$ ~ 2 cm^{-1}) and H (3,138 $\pm$ ~ 2 cm^{-1}), are, respectively, the peak frequencies of the LDA and HDA spectra (the dotted and dashed lines in the main part of **a**), whose difference corresponds to the gap in Fig. 2a. **b**, An example of the linear HDA/LDA combination. We calculate $\alpha I_{HDA} + (1 - \alpha) I_{LDA}$, where I_{HDA} and I_{LDA} are the HDA and LDA spectra (the dashed and dotted lines), respectively. The result of the fit to experimental data (broken line) agrees with the experimental data (grey dots).

© 2002 Nature Publishing Group

region with increasing temperature.

If the HDA–LDA transformation is first-order-like and therefore involves nucleation and growth of the new phase, the broadness of the low-temperature boundary region and its apparent narrowing at high temperatures are readily explained. That is, HDA will be less viscous at higher temperatures and LDA can thus grow more rapidly in the HDA region, resulting in a relatively narrow HDA–LDA boundary. The boundary region as a manifestation of HDA–LDA phase separation in the ice sample is also consistent with its disappearance in the 111-K experiment (Fig. 5). Moreover, this interpretation readily explains why many cracks appear in ice samples during their transformation, whereas densified silica glasses exhibit monotonic annealing behaviour without cracking (N. Kitamura, personal communication).

The HDA–LDA transformation has also been interpreted as spinodal decomposition, motivated by model calculations[21,22] that suggest that HDA around 120 K and 100 kPa might be unstable (as opposed to metastable) with respect to LDA. But because spinodal decompositions tend to be system-spanning[23], the observed heterogeneous propagation of the HDA–LDA transformation suggests that the theoretical calculations are not accurate; however, even though never observed so far, it might be possible that a low-temperature spinodal decomposition process lacking system-spanning characteristics occurs. At low temperatures and under out-of-equilibrium conditions, it is experimentally very difficult to differentiate clearly and unambiguously between the spinodal decomposition of an unstable state, and the kinetic transition of a metastable state. The detailed mechanism of the HDA–LDA first-order-like transformation thus remains uncertain.

The amorphous phases HDA and LDA easily crystallize on heating. It is thus practically very difficult to observe at temperatures above their expected glass-transition temperatures[10,19] the equilibrium first-order transformation anticipated to occur around ~0.2 GPa on the co-existence line of the low- and high-density liquid waters. But as these equilibrium conditions are approached, the phase separation between HDA and LDA should become more distinct. In fact, this is seen in experiments around ~135 K and ~0.2 GPa, which reveal LDA-to-HDA 'over-pressurization', HDA-

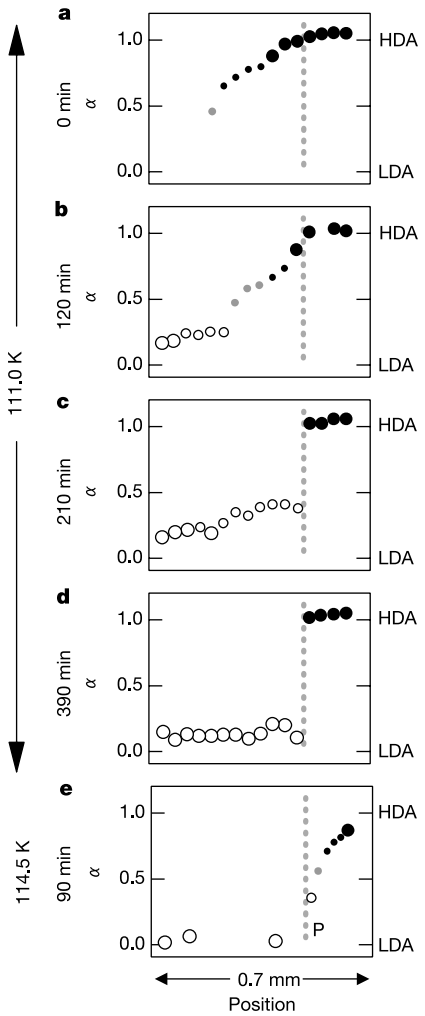

Figure 5 Phase changes in an amorphous sample at 111 K. The HDA–LDA transformation was initiated at 115 K and the sample then cooled to 111 K. Panels **a**–**e** show the α values along a line parallel to the transformation direction, analogous to the data shown in the right-hand panels in Fig. 3. The partly transformed sample is annealed for the indicated total period at 111 K and cooled for the Raman measurement at 25 K. The HDA–LDA transformation starts again when the sample is re-heated to 114.5 K. A crack grows with time at point P.

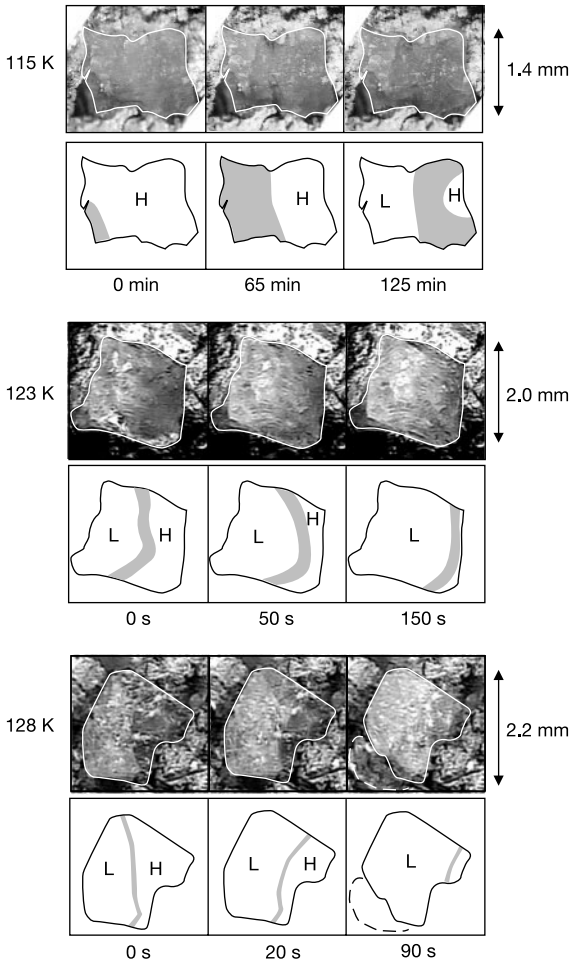

Figure 6 Visual observations of the transformations at 115, 123 and 128 K. Transformations proceed from left to right; times since taking the leftmost image are shown. The boundary region (the grey zone) in the 115-K images is identified using Raman measurements (Fig. 3). The location and width of the boundary regions in the samples transforming at 123 K and 128 K are visually inferred from the boundary between the densely cracked part (white area) and the uncracked part (black area), and are thus unlikely to correspond exactly to the shape given in the schematic figures. The samples just before and just after the 123-K and 128-K transformations are identified by Raman measurements as HDA (H) and LDA (L), respectively. The123-K sample shown transformed several times quicker than the usual samples at this temperature. The broken line shows the ice separated by a crack. The temperature (or time) at which HDA starts to change triggers the whole transformation, and varies between experiments; however, it can become roughly constant; for example, it occurs at 115 ± ~ 0.5 K in well-annealed HDA in a roughly one-hour timescale.

© 2002 Nature Publishing Group

to-LDA 'over-depressurization' and a narrow pressure hysteresis in the reversible transformation of the two phases[7,8].

Taken together, our findings strongly argue for the HDA–LDA transformation being a first-order phase transformation. Structurally, HDA and LDA resemble[24–27] high-density liquid water (HDL) and low-density liquid water (LDL), respectively, and the present results thus also support the liquid–liquid critical-point theory, which holds that HDL and LDL transform into each other through a discontinuous, first-order process. Finally, we note that a clear polyamorphic phase separation has already been observed in the Al_2O_3–Y_2O_3 system[28,29], and may be seen in other network-forming amorphous materials[30,31]. □

Received 5 July; accepted 3 September 2002; doi:10.1038/nature01106.

1. Debenedetti, P. G. One substance, two liquids? *Nature* **392,** 127–129 (1998).
2. Sastry, S., Debenedetti, P. G., Sciortino, F. & Stanley, H. E. Singularity-free interpretation of the thermodynamics of supercooled water. *Phys. Rev. E* **53,** 6144–6154 (1996).
3. Rebelo, L. P. N., Debenedetti, P. G. & Sastry, S. Singularity-free interpretation of the thermodynamics of supercooled water. II. Thermal and volumetric behavior. *J. Chem. Phys.* **109,** 626–633 (1998).
4. Poole, P. H., Sciortino, F., Essmann, U. & Stanley, H. E. Phase behaviour of metastable water. *Nature* **360,** 324–328 (1992).
5. Franzese, G. & Stanley, H. E. Liquid-liquid critical point in a Hamiltonian model for water: analytic solution. *J. Phys. Condens. Matter* **14,** 2201–2209 (2002).
6. Floriano, M. A., Handa, Y. P., Klug, D. D. & Whalley, E. Nature of the transformations of ice I and low-density amorphous ice to high-density amorphous ice. *J. Chem. Phys.* **91,** 7187–7192 (1989).
7. Mishima, O., Takemura, K. & Aoki, K. Visual observations of the amorphous-amorphous transition in H_2O under pressure. *Science* **254,** 406–408 (1991).
8. Mishima, O. Reversible first-order transition between two water amorphs at ~0.2 GPa and ~135 K. *J. Chem. Phys.* **100,** 5910–5912 (1994).
9. Moynihan, C. T. *Ann. NY Acad. Sci.* **484,** 94 (1986); **484,** 287 (1986).
10. Mishima, O. Relationship between melting and amorphization of ice. *Nature* **384,** 546–549 (1996).
11. Suzuki, Y., Takasaki, Y., Tominaga, Y. & Mishima, O. Low-frequency Raman spectra of amorphous ices. *Chem. Phys. Lett.* **319,** 81–84 (2000).
12. Loerting, T. *et al.* A second distinct structural "state" of high-density amorphous ice at 77 K and 1 bar. *Phys. Chem. Chem. Phys.* **3,** 5355–5357 (2001).
13. Klug, D. D., Mishima, O. & Whalley, E. Raman spectrum of high-density amorphous ice. *Physica B* **139 & 140,** 475–478 (1986).
14. Tulk, C. A. *et al.* Structural studies of several distinct metastable forms of amorphous ice. *Science* **297,** 1320–1323 (2002).
15. Sivakumar, T. C., Schuh, D., Sceats, M. G. & Rice, S. A. The 2500–4000 cm^{-1} Raman and infrared spectra of low density amorphous solid water and of polycrystalline ice I. *Chem. Phys. Lett.* **48,** 212–218 (1977).
16. Handa, Y. P., Mishima, O. & Whalley, E. High-density amorphous ice. III. Thermal properties. *J. Chem. Phys.* **84,** 2766–2770 (1986).
17. Klug, D. D., Mishima, O. & Whalley, E. High-density amorphous ice. IV. Raman-spectrum of the uncoupled O-H and O-D oscillators. *J. Chem. Phys.* **86,** 5323–5328 (1987).
18. Gromitskaya, E. L., Stal'gorova, O. V., Brazhkin, V. V. & Lyapin, A. G. Ultrasonic study of the nonequilibrium pressure-temperature diagram of H_2O ice. *Phys. Rev. B* **64,** 094205 (2001).
19. Mishima, O. & Suzuki, Y. Vitrification of emulsified liquid water under pressure. *J. Chem. Phys.* **115,** 4199–4202 (2001).
20. Balagurov, A. M. *et al.* Neutron-diffraction study of phase-transitions of high-pressure metastable ice-VIII. *JETP Lett.* **53,** 30–34 (1991).
21. Poole, P. H. *et al.* Effect of hydrogen bonds on the thermodynamic behavior of liquid water. *Phys. Rev. Lett.* **73,** 1632–1635 (1994).
22. Truskett, T. M., Debenedetti, P. G. & Sastry, S. A single-bond approach to orientation-dependent interactions and its implications for liquid water. *J. Chem. Phys.* **111,** 2647–2656 (1999).
23. Debenedetti, P. G. *Metastable Liquids* (Princeton Univ. Press, 1996).
24. Floriano, M. A., Whalley, E., Svensson, E. C. & Sears, V. F. Structure of high-density amorphous ice by neutron diffraction. *Phys. Rev. Lett.* **57,** 3062–3064 (1986).
25. Bellissent-Funel, M.-C. & Bosio, L. A neutron scattering study of liquid D_2O under pressure and at various temperatures. *J. Chem. Phys.* **102,** 3727–3735 (1995).
26. Soper, A. K. & Ricci, M. A. Structures of high-density and low-density water. *Phys. Rev. Lett.* **84,** 2881–2884 (2000).
27. Finney, J. L. *et al.* Structures of high and low density amorphous ice by neutron diffraction. *Phys. Rev. Lett.* **88,** 225503 (2002).
28. Aasland, S. & McMillan, P. F. Density-driven liquid–liquid phase separation in the system Al_2O_3–Y_2O_3. *Nature* **369,** 633–636 (1994).
29. Wilding, M. C. & McMillan, P. F. Polyamorphic transitions in yttria-alumina liquids. *J. Non-Cryst. Solids* **293–295,** 357–365 (2001).
30. Katayama, Y. *et al.* A first-order liquid–liquid phase transition in phosphorus. *Nature* **403,** 170–173 (2000).
31. Deb, S. K., Wilding, M., Somayazulu, M. & McMillan, P. F. Pressure-induced amorphization and an amorphous–amorphous transition in densified porous silicon. *Nature* **414,** 528–530 (2001).

Acknowledgements We thank S. Sastry and P. G. Debenedetti for discussions and comments, and N. Kitamura for information on silica glass.

Competing interests statement The authors declare that they have no competing financial interests.

Correspondence and requests for information should be addressed to O.M. (e-mail: mishima.osamu@nims.go.jp).

Directly measured mid-depth circulation in the northeastern North Atlantic Ocean

A. S. Bower*, B. Le Cann†, T. Rossby‡, W. Zenk§, J. Gould‖, K. Speer¶ P. L. Richardson*, M. D. Prater‡ & H.-M. Zhang#‡

* *Woods Hole Oceanographic Institution, Woods Hole, Massachusetts 02543, USA*
† *Laboratoire de Physique des Océans, CNRS, UFR Sciences, BP809, 29285 Brest, France*
‡ *Graduate School of Oceanography, University of Rhode Island, Kingston, Rhode Island 02881, USA*
§ *Institut für Meereskunde, Christian-Albrechts-Universität, D-24105 Kiel, Germany*
‖ *Southampton Oceanography Centre, Empress Dock, Southampton SO14 3ZH, UK*
¶ *Department of Oceanography, Florida State University, Tallahassee, Florida 32306, USA*

The circulation of water masses in the northeastern North Atlantic Ocean has a strong influence on global climate owing to the northward transport of warm subtropical water to high latitudes[1]. But the ocean circulation at depths below the reach of satellite observations is difficult to measure, and only recently have comprehensive, direct observations of whole ocean basins been possible[2–4]. Here we present quantitative maps of the absolute velocities at two levels in the northeastern North Atlantic as obtained from acoustically tracked floats. We find that most of the mean flow transported northward by the Gulf Stream system at the thermocline level (about 600 m depth) remains within the subpolar region, and only relatively little enters the Rockall trough or the Nordic seas. Contrary to previous work[5,6], our data indicate that warm, saline water from the Mediterranean Sea reaches the high latitudes through a combination of narrow slope currents and mixing processes. At both depths under investigation, currents cross the Mid-Atlantic Ridge preferentially over deep gaps in the ridge, demonstrating that sea-floor topography can constrain even upper-ocean circulation patterns.

Warm, subtropical waters are transported to the northern North Atlantic Ocean, mainly by the Gulf Stream and its poleward extension, the North Atlantic Current (NAC), where they are cooled and transformed into the intermediate and deep water masses that spread throughout the global ocean[1]. The pathways and speeds of the currents in this region directly affect the magnitude of this thermohaline circulation, but our ability to accurately measure them has suffered from a lack of widespread direct velocity observations. As part of a large international effort to directly observe the circulation throughout this region using floats[2], several research groups from the USA, the UK, Germany and France recently collaborated in a major initiative to measure the absolute velocity at two levels in the northeastern North Atlantic using acoustically tracked subsurface floats[2,7–9] (Fig. 1). Here we present a quantitative view of the mid-depth circulation in this region and highlight some unexpected results.

Figure 2 shows the mean potential temperature (θ) distribution at the two float levels from historical data[10], and sets the hydrographic context for the velocity observations. At the upper level, the warm subtropical thermocline waters spread northward mainly in the northeastern North Atlantic. Two sources for this warm water have been proposed[5,6,11]: the warm, salty Mediterranean Water in the southeast ($\theta > 10\,^{\circ}C$) that enters the North Atlantic through the Strait of Gibraltar, and the water transported by the Gulf Stream and

Present address: National Climatic Data Center, NOAA, Asheville, North Carolina 28801, USA.

© 2002 Nature Publishing Group